Theoretical Chemistry Accounts (2022) 141:77
https://doi.org/10.1007/s00214-022-02938-x

RESEARCH

Computational investigation on mechanisms and kinetics of gas-phase reactions of 4-hydroxy-2-pentanone (4H2P) with hydroxyl radicals and subsequent reactions of $CH_3C(O)CH_2C^{\cdot}(OH)CH_3$ radical

Kanika Guleria[1] · Ranga Subramanian[1]

Received: 17 August 2022 / Accepted: 7 November 2022 / Published online: 17 November 2022

Abstract
The mechanistic, thermochemical, and kinetic study of the 4-hydroxy-2-pentanone (4H2P) + OH radical reaction is performed for the first time by employing quantum theoretical calculations. The potential energy diagram was evaluated for five possible reaction pathways at the CCSD(T)/cc-pVTZ//BH&HLYP/cc-pVTZ level of theory. Theoretical rate coefficients of five abstraction pathways are computed as a function of temperature (210–350 K) utilizing the canonical variational transition state theory (CVT) with small-curvature tunneling (SCT). A three-parameter modified Arrhenius equation is used to fit rate coefficients. The thermodynamic quantities like reaction enthalpy and Gibbs free energy are calculated at the BH&HLYP/cc-pVTZ level of theory. According to thermodynamic analysis, the hydrogen abstraction from the –CH group adjacent to the hydroxyl group occurs more favorably and is the dominant pathway with minimum barrier height. The structure–activity relationship is explored by comparing rate coefficients of the titled reaction with the literature values of similar species. The subsequent fate of the alkyl radical ($CH_3C(O)CH_2C^{\cdot}(OH)CH_3$) is further studied in a NO-rich environment resulting in the formation of acetone, NO_2, and oxygen as the major final products.

Keywords Hydroxyketone · Potential energy surface · CVT/SCT · Branching ratio · Atmospheric lifetime · Alkyl radical

1 Introduction

Carbonyl compounds are widely spread atmospheric key components formed in the atmosphere by oxidation of volatile organic compounds (VOCs) emitted from biogenic and anthropogenic sources [1, 2]. They comprise a prominent class of organics released directly into the atmosphere. They are used in various industrial processes, including producing dyes, chloroform, fragrances, flavorings, and plastics, as well as solvents for resins, lacquers, and cellulose [3, 4]. They serve as fuel additives to lower soot emissions and fuel tracers for evaluating fuel qualities [5–8]. Volatile organic compounds (VOCs) are critical in the atmosphere because they directly connect with air quality and climate change [9–11]. Carbonyl compounds significantly affect urban air pollution and atmospheric chemistry. These carbonyl compounds extensively contribute to forming free radicals involved in the oxidation of hydrocarbons [12]. They are crucial intermediates in the creation of aerosols and serve as the building blocks for other oxidants like ozone, nitric acid, and peroxyacyl nitrates (PANs) [13].

Multifunctional ketones like hydroxyketones are hydroxyl and carbonyl group-containing compounds representing a significant class of oxygenated Volatile Organic Compounds (OVOCs) in the atmosphere. They are used in various industrial sectors, mainly in food [14], solvents, and pharmaceutical synthesis [15]. Hydroxyketones can either be released into the atmosphere as biogenic [16, 17] or anthropogenic pollutants [18] or formed by oxidation of alkanes, alkenes, and other oxygenated compounds [19, 20]. Like other carbonyl compounds, hydroxyketones are removed from the atmosphere in many possible ways like photolysis by solar radiation and oxidation by atmospheric oxidants like hydroxyl (OH), nitrate (NO_3) radicals, ozone (O_3) molecules, and. chlorine (Cl) atoms. The hydroxyl radical (OH) is the most reactive among these species, influencing various atmospheric chemical processes.

✉ Ranga Subramanian
ranga@iitp.ac.in

[1] Department of Chemistry, Indian Institute of Technology Patna, Patna 801103, India

Therefore, studying OH radical reaction with hydroxyketones is necessary to assess their significance in air pollution. These hydroxyketones reactions have recently received significant attention from experimental and theoretical research groups. Following this, we have studied the oxidation reaction of 4-hydroxy-2-pentanone (4H2P) with OH radical. 4H2P was found to be a biomass-derived molecule produced significantly through a distinct method than other hydroxyketones [21]. Based on the literature survey, no theoretical or experimental study has been reported till now for the 4H2P + OH reaction.

This paper provides the results of the first theoretical investigation of the kinetics and mechanism of 4H2P + OH radical reactions. This work's main objective is to better understand the studied reaction's importance as a removal process of 4H2P in the atmosphere. Therefore, we used computational tools to study the plausible mechanism and thermochemistry and obtain rate coefficients of various pathways of the titled reaction in the 210–350 K temperature range. The rate coefficient value was then used to calculate the atmospheric lifetime of 4H2P. Additionally, secondary organic aerosols (SOAs), which negatively impact the climate and humans, are produced as a byproduct of the oxidation reaction of ketones like acetone and pentanone with atmospheric oxidants [22–25]. Therefore, the manuscript also discusses the subsequent reaction mechanisms of the product produced in the reaction's pathway and the formation of SOA.

2 Computational details

All reaction species involved in hydrogen abstraction pathways were optimized in gas-phase using second-order Møller–Plesset perturbation (MP2) [26] theory and hybrid meta-density functional, Becke-Half-and-Half-LYP (BH&HLYP) [27]. Dunning's correlation-consistent polarized valence triple zeta (cc-pVTZ) basis set was used for geometrical optimization purposes [28]. In the previous studies of hydrogen abstraction reactions, the BH&HLYP method is trustworthy for evaluating optimized geometries and frequencies of reaction species [29–31]. $< S^2 >$ values given in Table S5 in the Supplementary Information (SI) evince the absence of spin contamination in various reaction species at the BH&HLYP/cc-pVTZ level of theory. We performed computations at BH&HLYP and MP2 levels with cc-pVXZ basis sets and then extrapolated to the complete basis set (CBS) limit to refine energies. We used Helgaker relation [32, 33] to carry out CBS extrapolations, which are given as

$$E_X = E_{CBS} + AX^{-3} \quad (1)$$

where E_X is the energy with X, that is 2, 3, 4, and 5 for cc-pVXZ basis sets, E_{CBS} is the CBS energy limit, and A is the fitting parameter. We did harmonic vibrational frequency analysis to understand the characteristics of stationary points on the potential energy diagram. Minima were defined as stationary points with only positive frequencies, and the appearance of one imaginary frequency verified the transition state. To validate the connectivity of transition states to their respective reactants and products, we performed intrinsic reaction coordinate (IRC) [34, 35] calculations at both theoretical methods. The minimum energy path (MEP) is obtained for further kinetic calculations at the BH&HLYP/cc-pVTZ level with a 0.1 Bohr gradient step size. Along the MEP, energy derivatives such as hessians and gradients are also calculated.

The rate coefficients depend on energy barriers, so higher theoretical calculations are performed to obtain barrier height values accurately. Using BH&HLYP/cc-pVTZ optimized geometries, we calculated single-point energy at coupled-cluster single-double and perturbative triples (CCSD(T)) [36] method with cc-pVTZ basis set to achieve a more accurate energetics. T1 diagnostic [37, 38] values given in Table S6 in the Supplementary Information (SI) are evaluated at the CCSD(T)/cc-pVTZ level and are clearly within the acceptable limit (0.045). Hence, the CCSD(T) single reference wave function is appropriate here. The IRC routes, vibrational movements, and molecular geometries were all visualized using the GaussView software [39]. Using the quantum chemistry code Gaussian16, all calculations involving electronic structure and energy were carried out [40].

All rate coefficient calculations were performed by utilizing the POLYRATE 2017-C program [41]. Utilizing variational transition state theory (VTST) and the interpolated single point energy (ISPE) method, the rate coefficients of each reaction pathway of the titled reaction are calculated. The rate coefficients are computed utilizing canonical variational transition state theory (CVT) in the 210–350 K temperature range [42–44]. For tunneling corrections, zero curvature tunneling (ZCT) [44–48] and small curvature tunneling (SCT) methods are employed [49, 50]. By minimizing the dividing surface s, the canonical variational theory rate coefficients($k^{\mathrm{CVT}}(T)$) [30, 51–53] are derived and can be written as:

$$k^{\mathrm{CVT}}(T) = \min k^{GT}(T, s) \quad (2)$$

$$k^{\mathrm{GT}}(T, s) = \frac{\sigma k_B T}{h} \frac{Q^{GT}(T, s)}{\phi^R(T)} \exp\left(-\frac{V_{\mathrm{MEP}}^{\mathrm{CVT}}(s)}{k_B T} \right) \quad (3)$$

where $k^{\mathrm{GT}}(T, s)$ denotes the generalized transition state theory rate coefficient at s, k_B is the Boltzmann constant $= 1.38 \times 10^{-23}$ J K^{-1}, T is the temperature, h is the Planck's constant $= 6.63 \times 10^{-34}$ J Hz^{-1}, and σ is the symmetry factor considered as unity. $Q^{GT}(T,s)$ is the partition function of the generalized transition state at s. $\phi^R(T)$ is the partition function of reactants per unit volume and $V_{MEP}^{CVT}(s)$ is the potential energy at point s, along the minimum energy path. While calculating electronic partition functions, the $^2\Pi_{3/2}$ and $^2\Pi_{1/2}$ electronic states of the OH radical are taken into account with a splitting of 140 cm^{-1}. By multiplying the CVT rate coefficient by a transmission coefficient κ_T, the tunneling effect is calculated. Transmission coefficient κ_T is computed by using two semiclassical tunneling approximations. One is the minimum energy path semiclassical adiabatic ground state (MEPSAG) method, also called zero-curvature tunneling (ZCT) approximation. ZCT approximation assumes that the reaction path has negligible curvature, so the tunneling path coincides with it. It neglects the contribution of multidimensional reaction-path curvature.

Another tunneling approximation is the centrifugal dominant slight curvature semiclassical adiabatic ground state (CD-SCSAG) method. This method is also called small-curvature tunneling (SCT) approximation. When the reaction path possesses curvature, the tunneling occurs on the concave side of the MEP [54–59]. CD-SCSAG method is a generalization of the Marcus-Coltrin approximation [59] in which the tunneling path is distorted from the MEP out to a concave-side vibrational turning point in the direction of the internal centrifugal force [49]. This method is based on the vibrationally adiabatic assumption and the assumption that the curvature of the reaction path in inertial coordinates is small [60].

ZCT and SCT keywords are given in the POLYRATE input file to get the transmission coefficient κ_T and tunneling corrected rate coefficients in the output file. Mainly geometries, frequencies, and force constants of reactants, transition states, and products, along with other keywords, are given in the POLYRATE input file and partition functions ($Q^{GT}(T,s)$, and $\phi^R(T)$), potential energy ($V_{MEP}^{CVT}(s)$), transmission coefficients (κ_T), and tunneling corrected rate coefficients ($k_{CVT/ZCT}$ and $k_{CVT/SCT}$) are obtained in the POLYRATE output file along with other results. A brief explanation of how the POLYRATE program calculates partition functions ($Q^{GT}(T,s)$, and $\phi^R(T)$) and transmission coefficients (κ_T) is given in the Supplementary Information (SI).

Modified Arrhenius equation is used to fit CVT/SCT rate coefficients in the temperature range of 210–350 K with the help of Origin2018 software [61].

$$k = AT^n \exp\left(\frac{-E_a}{RT}\right) \tag{4}$$

Here k = CVT/SCT rate coefficient values in the 210–350 K temperature range, T = 210–350 K, and R is the universal gas constant of 1.98 cal mol^{-1} s^{-1}. With the help of these values, we fitted the modified Arrhenius equation in the Origin2018 software and got the values of Arrhenius prefactor (A), energy barrier (E_a), and temperature exponent (n). The temperature exponent n arises from the temperature dependence of the Arrhenius prefactor. In the case of the famous Arrhenius theory, n = zero and n = 1/2 in the collision theory of gases for bimolecular gas phase reactions. In transition state theory, n is one or greater depending on the number of reacting species involved in the geometry of the activated complex [62].

The VTST-ISPE approach is utilized to evaluate temperature-dependent rate coefficients [63]. In this method, frequencies, stationary point geometries, and first derivatives were computed at the BH&HLYP/cc-pVTZ theoretical level. Reaction energies and barrier heights were improved by performing computations at a higher CCSD(T)/cc-pVTZ level.

3 Results and discussion

3.1 Optimized structures of stationary points

Figure 1 shows the optimized geometries of all stationary points involved in five hydrogen abstraction pathways of the 4H2P + OH reaction. Bond lengths and angles at BH&HLYP/cc-pVTZ and MP2/cc-pVTZ levels are displayed in Fig. 1. These two theoretical approaches are used to calculate vibrational frequencies. Table S1 in the Supplementary Information (SI) illustrates scaled vibrational frequencies accompanying limited experimental values. Each transition state has an imaginary frequency corresponding to the stretching modes of coupling breaking and forming bonds.

Hydrogen abstraction from –C(O)CH_3 group (1), from –CH_2 group (2), from –CH group (3), from –OH group (4), and from –CH_3 group (5) comprises five reaction pathways of the 4H2P + OH reaction as follows:

$CH_3C(O)CH_2CH(OH)CH_3$ + OH → $CH_2C(O)CH_2CH(OH)CH_3$ + H_2O (1)

$CH_3C(O)CH_2CH(OH)CH_3$ + OH → $CH_3C(O)CHCH(OH)CH_3$ + H_2O (2)

$CH_3C(O)CH_2CH(OH)CH_3$ + OH → $CH_3C(O)CH_2C(OH)CH_3$ + H_2O (3)

$CH_3C(O)CH_2CH(OH)CH_3$ + OH → $CH_3C(O)CH_2CH(O)CH_3$ + H_2O (4)

$CH_3C(O)CH_2CH(OH)CH_3$ + OH → $CH_3C(O)CH_2CH(OH)CH_2$ + H_2O (5)

The abstraction reaction of 4H2P by OH radical starts by forming reactant complexes. Due to hydrogen bond interactions, all reactant complexes have lower energies than reactants, stabilizing them. The breaking C–H bond in TS1, TS2, TS3, and TS5 is lengthened by 13.24%, 13.47%, 18.48%, and 15.75% as compared to the equilibrium C–H bond distance

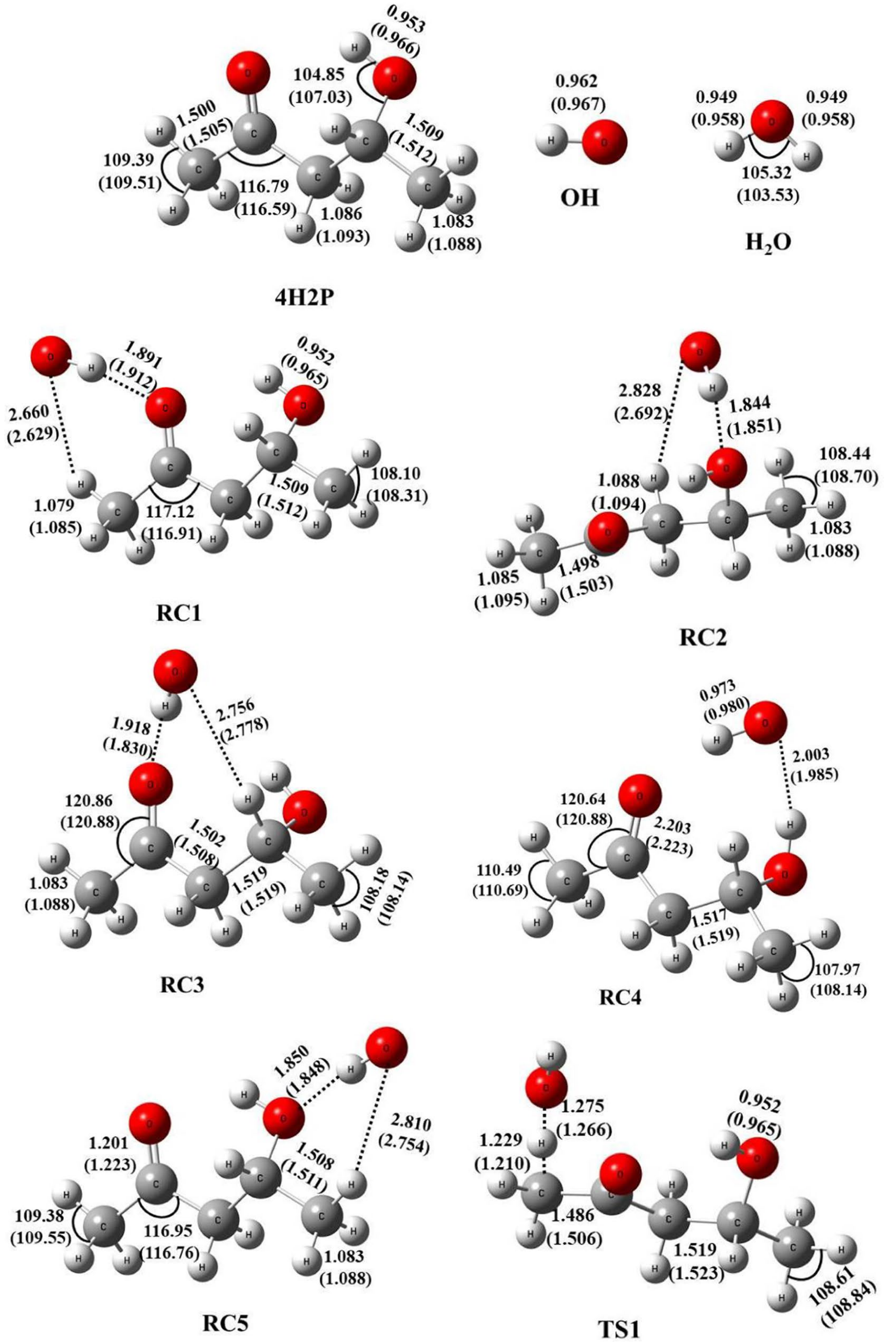

Fig. 1 Optimized geometries of reactants, reactant complexes, transition states, product complexes, and products of $CH_3C(O)CH_2CH(OH)CH_3 + OH$ reaction at BH&HLYP/cc-pVTZ and MP2/cc-pVTZ (in brackets) levels. Bond lengths are in angstroms, and angles are in degrees

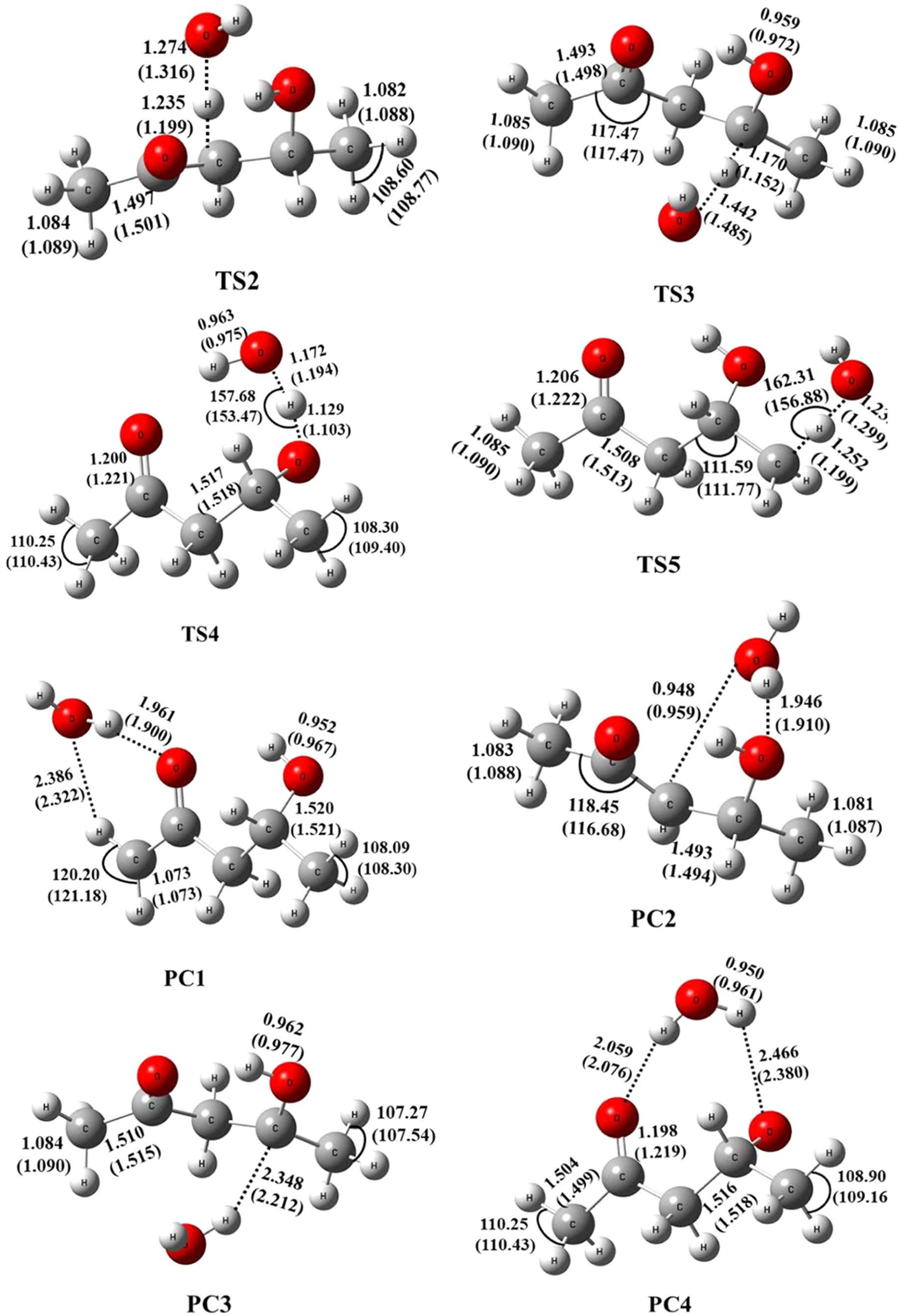

Fig. 1 (continued)

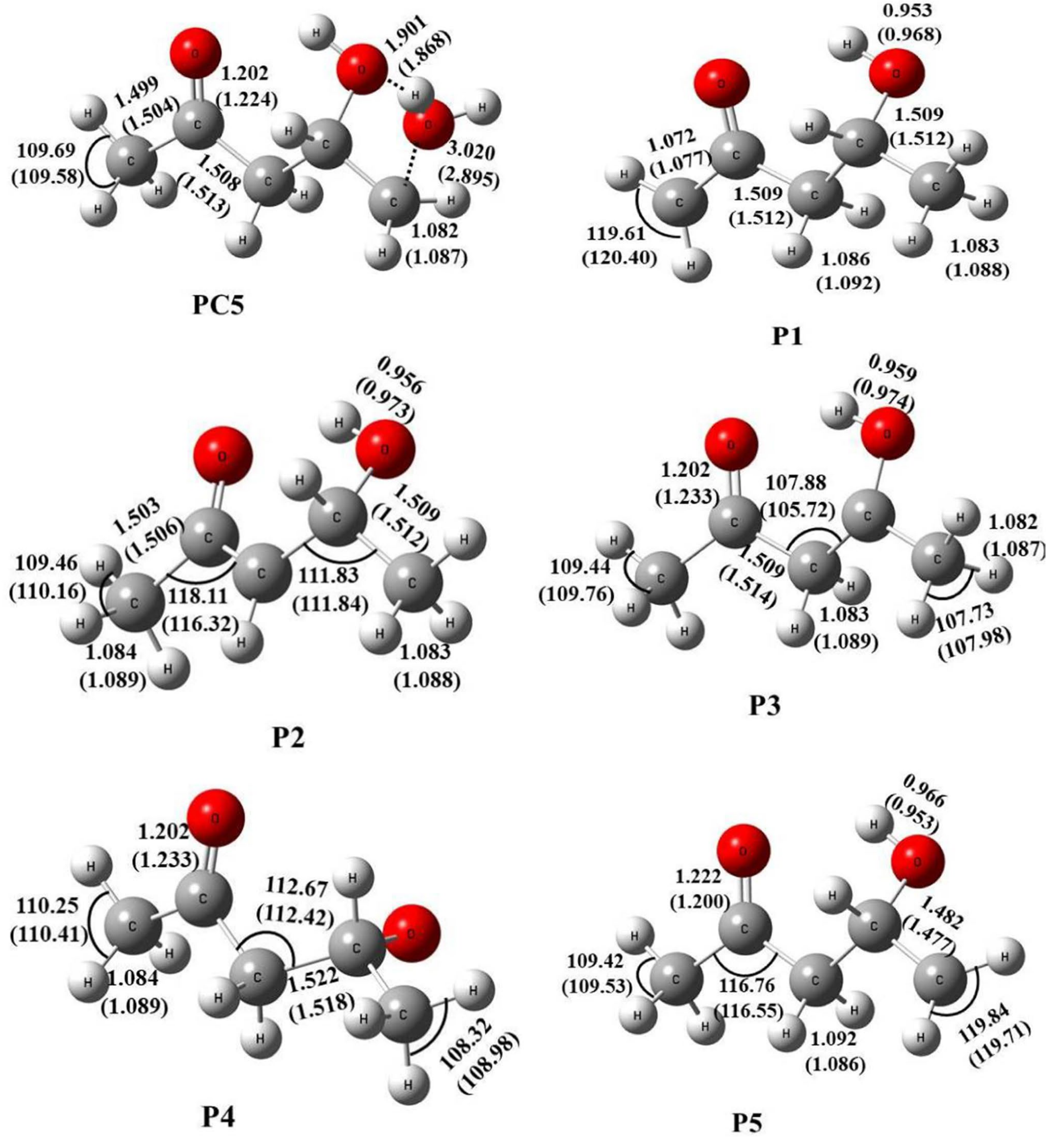

Fig. 1 (continued)

in 4H2P, respectively. The dissociating O–H bond length in TS4 increases by 7.52% compared to the equilibrium O–H bond length in 4H2P. Compared to the equilibrium O–H bond length in free H_2O molecule, the O–H bond in TS1, TS2, TS3, TS4, and TS5 is stretched by 34.41, 34.18, 51.92, 23.47, and 30.10%, respectively. It is evident from transition states TS1, TS2, TS3, TS4, and TS5 that establishing bonds elongate more than breaking bonds do. All transition states are reactant-like according to Hammond's postulate [64], and reactions will progress through early transition states. Product complexes (PC1, PC2, PC3, PC4, and PC5) are

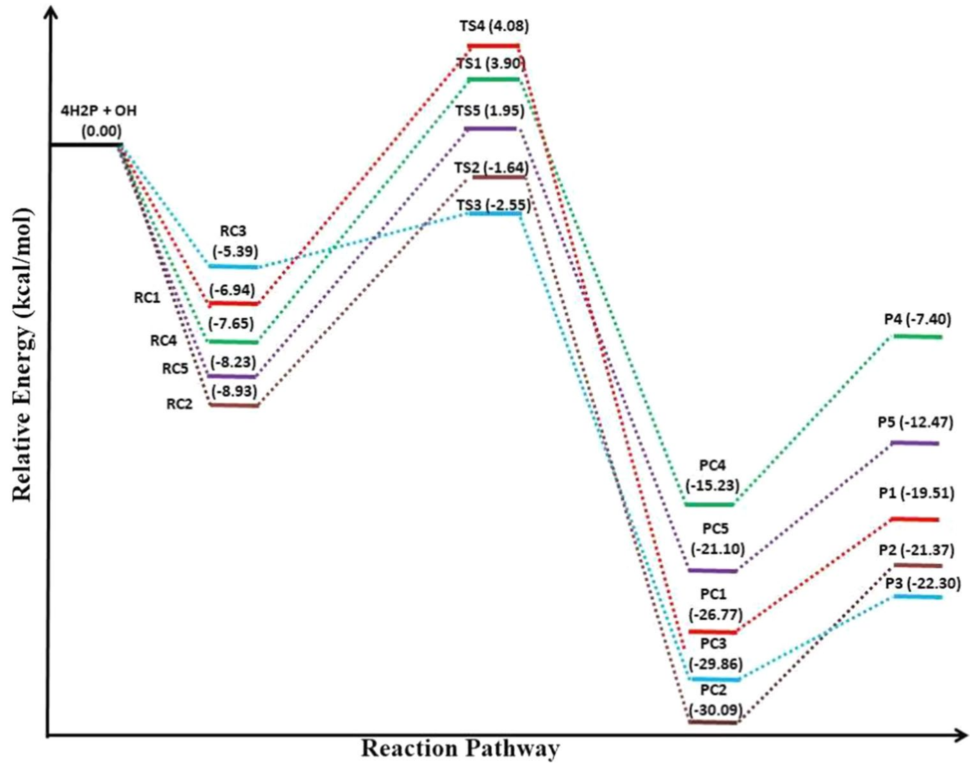

Fig. 2 Potential energy diagram of the 4H2P + OH reaction. Relative electronic energies (in kcal/mol) are computed at the CCSD(T)/cc-pVTZ//BH&HLYP/cc-pVTZ level

more energetically stable than their related products after overcoming potential barriers because of hydrogen bonding.

3.2 Reaction mechanisms and energetics

Figure 2 depicts the potential energy diagram for the 4H2P + OH reaction's five abstraction pathways. Reactants' energies are fixed to zero for reference. Relative energies are given in Table S3 in the Supplementary Information (SI). From Fig. 2, it can be visualized that the barrier height for reaction pathway 1 is 10.84 kcal/mol, 7.29 kcal/mol for reaction pathway 2, 2.84 kcal/mol for pathway 3, 11.73 kcal/mol for pathway 4, and 10.18 kcal/mol for pathway 5. Reaction pathway 3 has the lowest barrier height among all other reaction pathways. As a result, reaction pathway 3's rate coefficients will be higher than those of other reaction pathways.

The thermodynamic quantities like reaction enthalpies $\left(\Delta H^{\circ}_{298.15}\right)$ and Gibbs free energies $\left(\Delta G^{\circ}_{298.15}\right)$ of five reaction pathways are computed at the BH&HLYP/cc-pVTZ level of theory, and values are given in Table S4 in the Supplementary Information (SI). The reaction enthalpies values for 1, 2, 3, 4, and 5 reaction pathways are − 17.46, − 19.98, − 20.23, − 8.50, and − 10.54 kcal/mol, respectively. Based on these values, it can be gleaned that all reaction pathways are exothermic, with reaction pathway 3 being thermodynamically more favorable than the others. From $\left(\Delta G^{\circ}_{298.15}\right)$ values given in Table S4, we can conclude that all reaction pathways (1, 2, 3, 4, and 5) are spontaneous, having $\left(\Delta G^{\circ}_{298.15}\right)$ values − 18.35, − 21.97, − 21.90, − 10.41, and − 12.56 kcal/mol, respectively.

3.3 Rate coefficient calculations

Using canonical variational transition state theory (CVT), we estimated the 4H2P + OH reaction rate coefficients over the temperature range of 210–350 K. Zero curvature tunneling (ZCT) and small curvature tunneling (SCT) corrections are used to incorporate the tunneling effect. Figure 3a, b, c, d, and e displays the CVT, CVT/ZCT, and CVT/SCT rate coefficients of five abstraction pathways of the titled reaction. Tables S7-S11 in the Supplementary Information (SI) comprise all rate coefficient values.

The tunneling effect is defined as the ratio of CVT/SCT with CVT rate coefficients in Fig. 3a–e is significant for all reaction pathways across the temperature range. With temperature rise, the tunneling effect decreases. Figure 3f displays the CVT/SCT rate coefficients for each reaction pathway and the overall reaction, and Table S12 in the Supplementary Information (SI) provides the values. From Fig. 3f, we can conclude that reaction pathway 3 has faster rate coefficients than other reaction pathways. This outcome is compatible with energy barrier values, as reaction pathway 3's energy barrier is minimum among other reaction pathways.

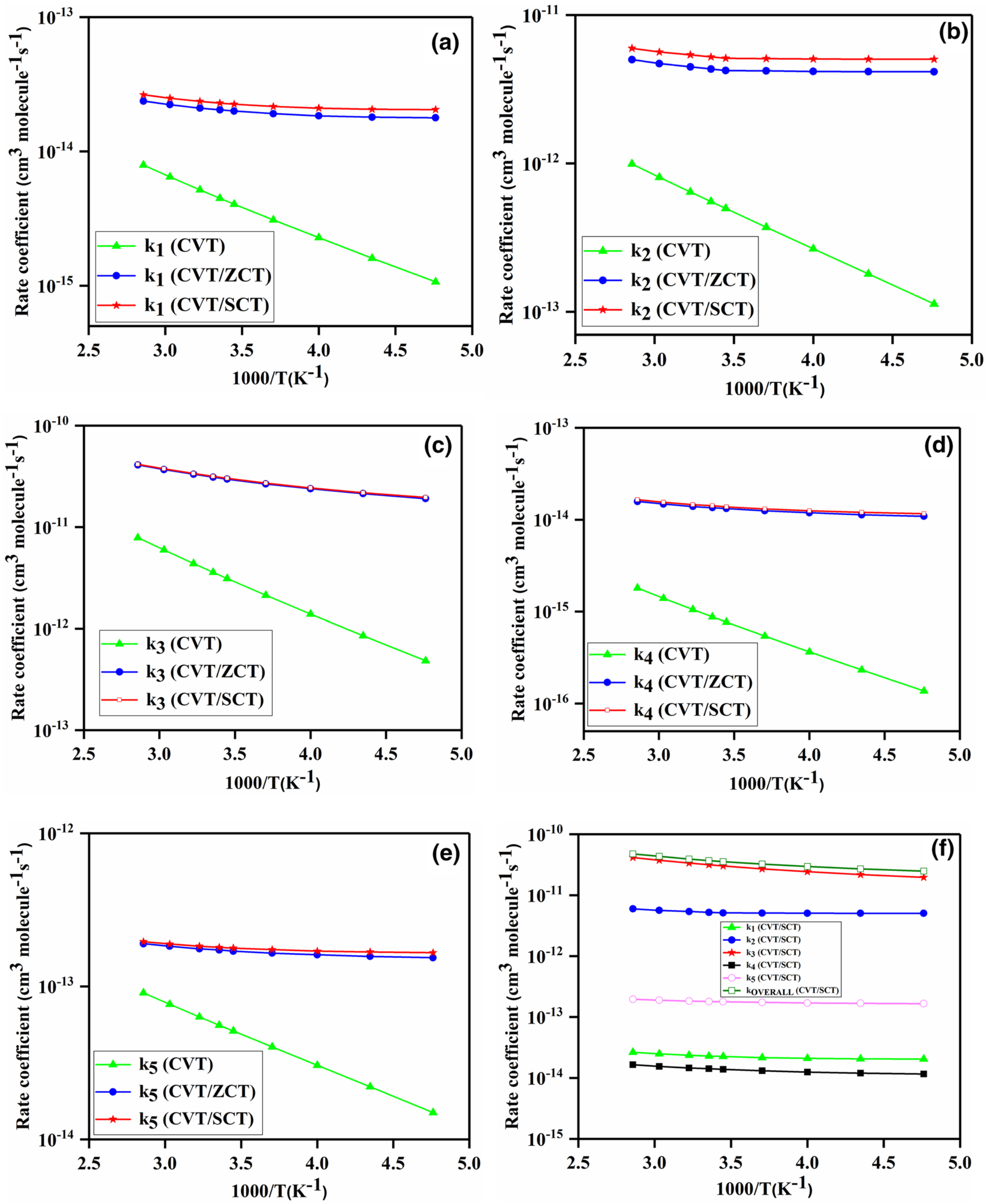

Fig. 3 CVT/SCT rate coefficients of reaction pathways 1 (3a), 2 (3b), 3 (3c), 4 (3d), 5 (3e) and overall reaction of 4H2P + OH (3f) at CCSD(T)/cc-pVTZ//BH&HLYP/cc-pVTZ level in the temperature range of 210–350 K

Modified Arrhenius parameters utilizing CVT/SCT rate coefficients of the five abstraction pathways and overall 4H2P + OH reaction are given in Table 1. Figure 4 shows the fitted Arrhenius plot, demonstrating that CVT/SCT rate coefficients exhibit a positive temperature dependency in the 210–350 K temperature range.

The negative and zero E_a values are found for all reaction pathways and overall reaction. Negative E_a values imply that reactants have attractive forces, and reaction initially proceeds via the formation of intermediate complexes [65]. This can be seen in the mechanism proposed for the titled reaction. Reactant complexes are found on the potential energy diagram in Fig. 2.

Table 1 Fitted modified Arrhenius parameters ($k = AT^n \exp(-E_a/RT)$) of all reaction pathways and overall 4H2P + OH reaction utilizing CVT/SCT rate coefficients at CCSD(T)/cc-pVTZ//BH&HLYP/cc-pVTZ level over the temperature range of 210–350 K

Reaction pathway	A (cm^3 $molecule^{-1}$ s^{-1})	n	E_a (kcal mol^{-1})
1	6.02×10^{-22}	2.71	− 1.17
2	7.41×10^{-20}	2.78	− 1.31
3	7.13×10^{-19}	2.87	− 0.74
4	8.80×10^{-21}	2.26	− 0.83
5	1.66×10^{-17}	1.45	− 0.60
Overall	2.17×10^{-19}	3.04	− 0.93

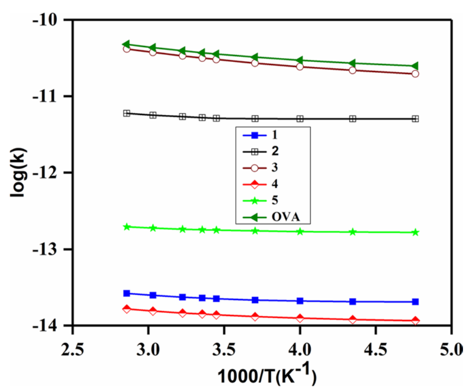

Fig. 4 The fitted Arrhenius plot of overall reaction and all reaction pathways of 4H2P + OH over the temperature range of 210–350 K

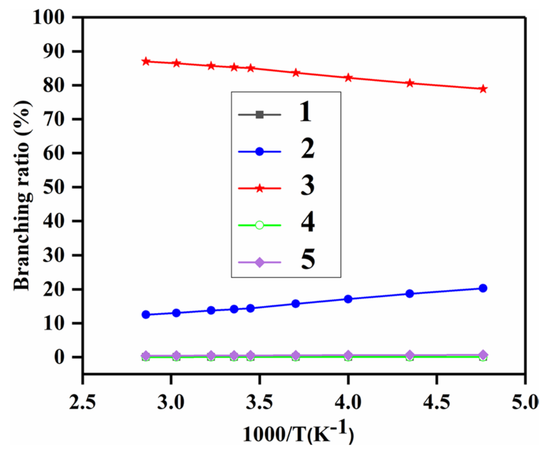

Fig. 5 The 4H2P + OH reaction calculated branching ratios over the temperature range of 210–350 K utilizing CVT/SCT rate coefficients

3.4 Branching ratio

The branching ratio is the ratio of the individual reaction pathway rate coefficient to the overall rate coefficient. We have calculated the branching ratio for all reaction pathways of the 4H2P + OH reaction, and values are given in Table S13 in the Supplementary Information (SI). The computed branching ratios for 1, 2, 3, 4, and 5 reaction pathway at 298 K are 0.06, 14.12, 85.30, 0.04, and 0.49%, respectively. From Fig. 5, it can be concluded that the branching ratios of reaction pathways 1, 4, and 5 are extremely low, and reaction pathway 3 is having highest branching ratio among all reaction pathways over the entire temperature range. The contribution from reaction pathway 3 is maximum, so it is the major pathway.

Table 2 provides an overview of the overall rate coefficients of the titled reaction and reactions of several similar hydroxyketones with OH radical at 298 K.

The oxidation reaction of 4H2P by OH radical is anticipated to occur through hydrogen abstraction, similar to other aliphatic ketones. According to our theoretical study, hydrogen abstraction advances mainly from the active methylene group (–CH group), i.e., reaction pathway (3), followed by the –CH_2 group and methyl group (–CH_3 group). Comparison of rate coefficients of 4H2P + OH reaction with that of other aliphatic ketones and hydroxyketones leads to the following trends:

- The rate coefficients of hydroxyketones + OH reaction are more significant than their corresponding ketones. Because hydroxyketones react with OH primarily through hydrogen abstraction of the weakest C-H bond of the -CH(OH) group, which is activated by the -OH substituent group. 4H2P + OH, 3-Hydroxy-2-Butanone + OH, and hydroxyacetone + OH reactions follow this trend compared to their corresponding ketones.
- Hydroxyketones with one tertiary hydrogen atom at the β position are more reactive toward OH oxidation than hydroxyketones with no β hydrogen atom. The OH functional group activates this tertiary hydrogen atom, which increases the rate coefficient value. This trend was followed by 4H2P when compared with 4-hydroxy-4-methyl-2-pentanone and 3-hydroxy-2-butanone when compared with 3-hydroxy-3-methyl-2-butanone.
- The reactivity of hydroxyketones toward OH radical increases with chain length. At room temperature, the rate coefficient increases from hydroxyacetone, 3-hydroxy 2-butanone, to 4-hydroxy 2-pentanone. The increase in rate coefficient values is due to an increase in the number of abstractable hydrogens as chain length increases.
- β-hydroxyketones are more reactive toward OH oxidation than α-hydroxyketones because of deactivating effect of the carbonyl group on α-carbon atoms. This trend can be seen in the case of 4-hydroxy-4-methyl-2-pentanone, as its rate coefficient values are higher than that of 3-hydroxy-3-methyl-2-butanone.

Table 2 Rate coefficients of the reactions of OH radicals with several ketones and hydroxyketones, including 4H2P at 298 K

Species	k_{OH} (cm^3 $molecule^{-1}$ s^{-1})	Technique	References
Acetone	$(2.16\pm0.16)\times10^{-13}$	Flash photolysis resonance fluorescence	Wallington and Kurylo [66]
	1.92×10^{-13}	Theory	Alvarez-Idaboy et al. [67]
Hydroxyacetone	$(3.02\pm0.28)\times10^{-12}$	Resonance fluorescence	Stevens et al. [68]
	3.15×10^{-12}	Theory	Galano [69]
2-Butanone	$(1.15\pm1.0)\times10^{-12}$	Flash photolysis resonance fluorescence	Wallington and Kurylo [66]
	3.5×10^{-12}	Theory	Gao et al. [70]
3-Hydroxy-2-Butanone	$(1.03\pm2.2)\times10^{-11}$	Relative rate (GC-FID)	Atkinson et al. [9]
	1.20×10^{-11}	Theory	Singh et al. [29]
3-Hydroxy-3-Methyl-2-Butanone	$(9.4\pm3.7)\times10^{-13}$	Relative rate (GC-FID)	Atkinson et al. [9]
	1.04×10^{-12}	Theory	El Dib et al. [30]
2-Pentanone	$(4.56\pm0.30)\times10^{-12}$	Relative rate-FTIR	Atkinson et al. [71]
	2.38×10^{-12}	Theory	Alvarez-Idaboy et al. [67]
4-Hydroxy-2-Pentanone	3.70×10^{-11}	Theory	This work
4-Hydroxy-4-Methyl-2-Pentanone	4.75×10^{-12}	Laser-induced fluorescence	Lakshmipathi et al. [53]
	2.88×10^{-12}	Theory	Lakshmipathi et al. [53]

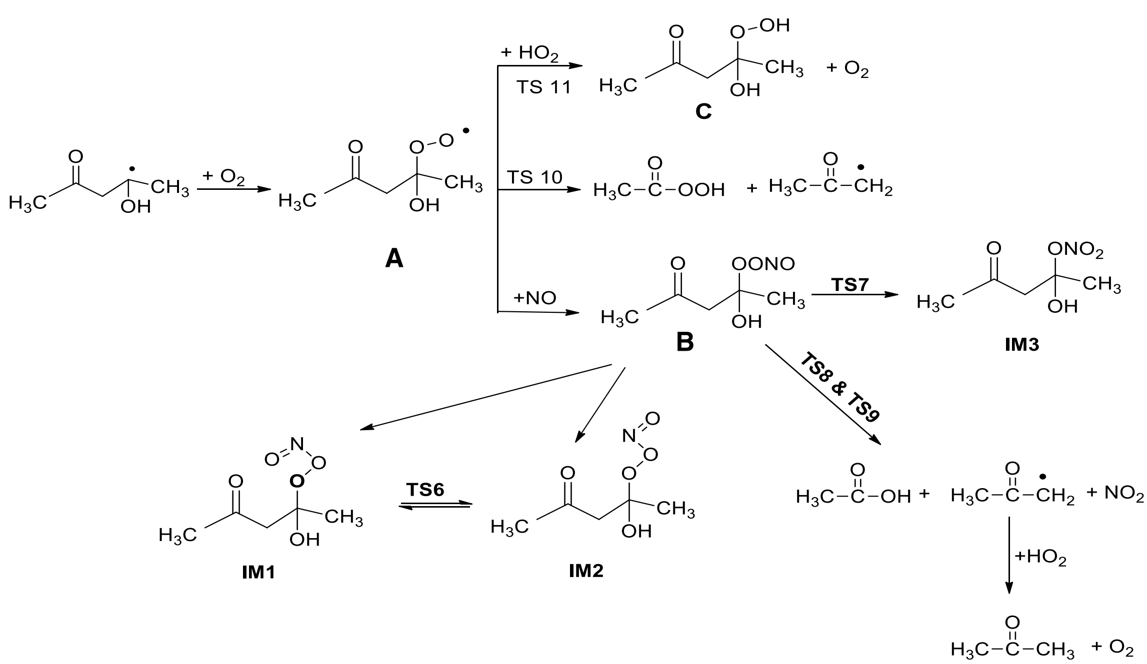

Scheme 1 Proposed mechanism of the consequent reactions of the $CH_3C(O)CH_2C(OO^{\cdot})(OH)CH_3$ radical

3.5 Secondary reactions of $CH_3C(O)CH_2C^{\cdot}(OH)CH_3$ radical

Thermodynamic and kinetics results reveal that pathway 3 is the most favorable, producing alkyl radical $CH_3C(O)CH_2C^{\cdot}(OH)CH_3$ and water. The degradation processes of $CH_3C(O)CH_2C^{\cdot}(OH)CH_3$ were further studied and are shown in Scheme 1. In the oxygen-abundant atmosphere, alkyl radical forms peroxide radical $CH_3C(O)CH_2C(OO^{\cdot})(OH)CH_3$ (A) by reacting with O_2 in the atmosphere through a barrierless pathway. Peroxide radicals are crucial in atmospheric chemistry. [10, 72–75]. The peroxide radical (A) undergoes a H-migration reaction to form acetonyl radical and peroxyacetic acid. Also, after reacting with HO_2, peroxide radical (A) forms $CH_3C(O)CH_2C(OOH)(OH)CH_3$ and O_2 via TS11.

According to Atkinson and Arey, the reaction of RO_2 with NO occurs predominantly in the atmosphere compared to other radicals [10]. Generally, the $RO_2 + NO$ reaction produces alkoxy radicals and NO_2. But in the present work,

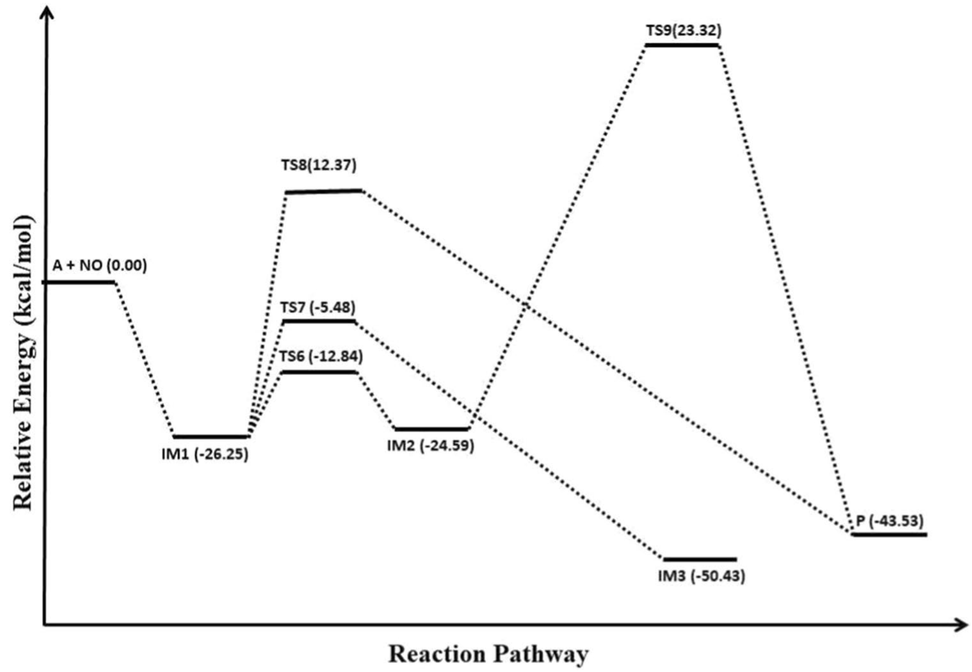

Fig. 6 Schematic potential energy diagram for the consequent pathways of the A + NO reaction at the CCSD(T)/cc-pVTZ//BH&HLYP/cc-pVTZ level

because of the poor stability of the alkoxy radical, while performing the NO_2 elimination reaction, the C–C bond will break. The peroxide radical (A) reaction with NO results in the formation of peroxynitrite (B). This peroxynitrite (B) has two forms, namely IM1(cis-$CH_3C(O)CH_2C(O_2NO)(OH)CH_3$ and IM2 trans-$CH_3C(O)CH_2C(O_2NO)(OH)CH_3$). IM1 isomerizes to form IM2 through TS6. IM1 and IM2 yield acetonyl radical and stable product acetic acid through TS8 and TS9, respectively, by eliminating NO_2. The acetonyl radical, after reacting with HO_2, yields acetone and oxygen molecule.

Secondary organic aerosols (SOA) account for the majority of aerosol mass present in the atmosphere. These SOA seriously affect air quality, atmospheric chemistry, and human health [22–25]. IM1 do tautomerization via TS7 to form IM3 ($CH_3C(O)CH_2C(ONO_2)(OH)CH_3$) which is an SOA that influences climate and people's life adversely.

The relative energies of various species are obtained at the CCSD(T)/cc-pVTZ//BH&HLYP/cc-pVTZ level. The transition state TS10 of the H-migration reaction has a barrier height of 45.86 kcal/mol. The enthalpy and Gibbs free energy associated with the H-migration reaction are 5.48 kcal/mol and − 8.73 kcal/mol, respectively, implying this reaction is endothermic and spontaneous. Transition state TS11 involved in A's reaction with HO_2 has a barrier height of 16.57 kcal/mol. This reaction has a − 34.27 kcal/mol ΔH value and − 32.46 kcal/mol ΔG value, demonstrating this reaction to be exothermic and spontaneous. The potential energy surface for the A + NO reaction is shown in Fig. 6. The $< S^2 >$ and T1 diagnostic values of the A + NO reaction species are listed in Tables S14 and S15 in the Supplementary Information (SI).

After reacting with NO, the peroxide radical (A) forms peroxynitrites IM1 and IM2, which have binding energies of − 26.25 and − 24.59 kcal/mol, respectively. IM1 can be transformed into IM2 and IM3 via TS6 and TS7 transition states with a barrier height of 20.77 and 13.41 kcal/mol, respectively. Barrier height values imply that IM1 and IM2 conversion is easier than IM1 and nitrate ester IM3 conversion. With respect to reactants, the energy of nitrate ester IM3 is -50.43 kcal/mol, and the exothermicity of this reaction is –38.83 kcal/mol, implying this reaction is exothermic. In addition, IM2 nitrite undergoes C–C and O–O bond scission via TS9 to form acetonyl radical, acetic acid, and NO_2. The barrier height of this reaction is 47.91 kcal/mol with a − 42.96 kcal/mol ΔH value, and ΔG for this reaction is − 44.50 kcal/mol. However, IM1 generates the same product via TS8 with an energy barrier of 38.62 kcal/mol. Hence, cis-form generates NO_2 more easily than trans-form. Therefore, acetone, NO_2, and oxygen are the final products of OH-initiated atmospheric oxidation of 4H2P.

4 Atmospheric implications

The atmospheric lifetimes of volatile organic compounds generally depend on the atmosphere's many physical and chemical processes. However, oxidizing species, including OH radicals, Cl atoms, O_3 molecules, and NO_3 radicals, are primarily responsible for removing volatile organic chemicals from the atmosphere. As OH radicals are considered the atmosphere's detergent, the reaction of 4H2P with OH radicals plays a significant role in determining atmospheric lifetime. So the atmospheric lifetime of 4H2P (τ_{eff}) can be calculated by assuming that it is removed from the atmosphere primarily by reaction with OH radicals and is given as:

$$\frac{1}{\tau_{eff}} = \frac{1}{\tau_{OH}} \tag{5}$$

where $\tau_{eff} \approx \tau_{OH} = \left(k_{OH} \times [OH]\right)^{-1}$, where τ_{OH} is the lifetime of 4H2P with OH radicals, k_{OH} is the rate coefficient of 4H2P with OH radicals, equal to 3.70×10^{-11} cm^3 $molecule^{-1}$ s^{-1}, and [OH] concentration $= 2.0 \times 10^6$ molecules cm^{-3} [76]. By utilizing all these values, the calculated lifetime for 4H2P is 3.75 h.

5 Conclusions

This work comprises the first mechanistic and chemical kinetic study of the 4H2P + OH reaction using density functional theory and canonical variational transition state theory. We have constructed the potential energy diagram of the titled reaction at the CCSD(T)/cc-pVTZ//BH&HLYP/cc-pVTZ level. All five pathways are exothermic and spontaneous as all have negative $\left(\Delta H^{\circ}_{298.15}\right)$ and $\left(\Delta G^{\circ}_{298.15}\right)$ values. The energy barrier for reaction pathway 3 is minimum among five possible pathways, so it is expected to have faster rate coefficients than other reaction pathways. In the temperature range of 210–350 K, rate coefficients were computed using canonical variational transition state theory (CVT) with small-curvature tunneling (SCT) correction. For all five reaction pathways, it is found that the tunneling effect exists significantly over the whole temperature range. The overall rate coefficient of the 4H2P + OH reaction at 298 K is calculated to be 3.70×10^{-11} cm^3 $molecule^{-1}$ s^{-1}. The calculated atmospheric lifetime of tested molecule 4H2P is very short (3.75 h). Both energetic and kinetic calculations reveal that the attack of OH radical occurs predominantly at the –CH position of the tested 4H2P molecule. Based on the thermodynamic study, it is also proposed that the hydrogen abstraction from the –CH group of the 4H2P molecule (reaction pathway 3) is the most favorable pathway to occur. The branching ratio study indicated that reaction pathway 3 has the maximum contribution to the overall rate coefficient as the branching ratio for reaction pathway 3 (85.30%) is the highest among other reaction pathways. Hence, it is the major reaction pathway. We hope our theoretical study of the titled reaction will provide helpful information for future experimental studies.

Supplementary Information The online version contains supplementary material available at https://doi.org/10.1007/s00214-022-02938-x.

Acknowledgements Kanika Guleria thanks the Indian Institute of Technology Patna for providing financial support and research facilities to accomplish this work.

Author contributions KG contributed to the conceptualization, methodology, analysis, and writing—original draft. RS contributed to writing—review and editing and supervision.

Funding This study was funded by Indian Institute of Technology, Patna.

Declarations

Conflict of interest The authors declare no competing interests.

References

1. Atkinson R (1986) Kinetics and mechanisms of the gas-phase reactions of the hydroxyl radical with organic compounds under atmospheric conditions. Chem Rev 86:69–201. https://doi.org/10.1021/cr00071a004
2. Atkinson R (1994) Gas-phase tropospheric chemistry of volatile organic compounds. J Phys Chem Ref Data 21:1–216. https://doi.org/10.1063/1.556012
3. Hudzik M, Bozzelli JW (2012) Thermochemistry and bond dissociation energies of ketones. J Phys Chem A 116:5707–5722. https://doi.org/10.1021/jp302830c
4. Sebbar N, Bozzelli J, Bockhorn H (2011) Thermochemistry and kinetics for 2-Butanone-1-yl radical ($CH_2 \cdot C(=O)CH_2CH_3$) reactions with O_2. J Phys Chem A 18:21–37. https://doi.org/10.1021/jp408708u
5. Hanson RK, Seitzman JM, Paul PH (1990) Planar laser-fluorescence imaging of combustion gases. Appl Phys B 50:441–454. https://doi.org/10.1007/BF00408770
6. Schulz C, Sick V (2005) Tracer-LIF diagnostics: quantitative measurement of fuel concentration, temperature and fuel/air ratio in practical combustion systems. Prog Energy Combust Sci 31:75–121. https://doi.org/10.1016/j.pecs.2004.08.002
7. Pepiot-Desjardins P, Pitsch H, Malhotra R, Kirby S, Boehman AL (2008) Structural group analysis for soot reduction tendency of oxygenated fuels. Combust Flame 154:191–205. https://doi.org/10.1016/j.combustflame.2008.03.017
8. Hong Z, Davidson D, Vasu S, Hanson R (2009) The effect of oxygenates on soot formation in rich heptane mixtures: a shock tube study. Fuel 88:1901–1906. https://doi.org/10.1016/j.fuel.2009.04.013
9. Aschmann SM, Arey J, Atkinson R (2000) Atmospheric chemistry of selected hydroxycarbonyls. J Phys Chem A 104:3998–4003. https://doi.org/10.1021/jp9939874
10. Atkinson R, Arey J (2003) Atmospheric degradation of volatile organic compounds. Chem Rev 103:4605–4638. https://doi.org/10.1021/cr0206420
11. Monks PS (2005) Gas-phase radical chemistry in the troposphere. Chem Soc Rev 34:376–395. https://doi.org/10.1039/B307982C
12. de Andrade M, Pinheiro H, Pereira P, de Andrade J (2002) Atmospheric carbonyl compounds: sources, reactivity, concentration levels, and toxicologic effects. Quím Nova 25:1117–1131. https://doi.org/10.1590/S0100-40422002000700013
13. Ciccioli P, Brancaleoni E, Frattoni M, Cecinato A, Brachetti A (1993) Ubiquitous occurrence of semi-volatile carbonyl

compounds in tropospheric samples and their possible sources. Atmos Environ A Gen Top 27:1891–2190. https://doi.org/10.1016/0960-1686(93)90294-9
14. Rivas B, Torre P, Manuel DJ, Perego P, Converti A, Carlos Parajó J (2003) Carbon material and bioenergetic balances of xylitol production from corncobs by debaryomyces hansenii. Biotechnol Prog 19:706–713. https://doi.org/10.1021/bp025794v
15. Ichikawa N, Sato S, Takahashi R, Sodesawa T (2005) Synthesis of 3-buten-2-one from 4-hydroxy-2-butanone over anatase-TiO_2 catalyst. Catal Commun 6:19–22. https://doi.org/10.1016/j.catcom.2004.10.004
16. Řezanka T, Libalova D, Votruba J, Viden I (1994) Identification of odorous compounds from Streptomyces avermitilis. Biotechnol Lett 16:75–78. https://doi.org/10.1007/BF01022627
17. Knudsen JT, Eriksson R, Gershenzon J, Ståhl B (2006) Diversity and distribution of floral scent. Bot Rev 72:1–120. https://doi.org/10.1663/0006-8101(2006)72[1:DADOFS]2.0.CO;2
18. Nishanth T, Praseed K, Rathnakaran K, Kumar MS, Krishna RR, Valsaraj K (2012) Atmospheric pollution in a semi-urban, coastal region in India following festival seasons. Atmos Environ 47:295–306. https://doi.org/10.1016/j.atmosenv.2011.10.062
19. Bethel HL, Atkinson R, Arey J (2003) Hydroxycarbonyl products of the reactions of selected diols with the OH radical. J Phys Chem A 107:6200–6205. https://doi.org/10.1021/jp027693l
20. Saunders SM, Jenkin ME, Derwent R, Pilling M (2003) Protocol for the development of the master chemical mechanism, MCM v3 (part A): tropospheric degradation of non-aromatic volatile organic compounds. Atmos Chem Phys 3:161–180. https://doi.org/10.5194/acp-3-161-2003
21. Chia M, Schwartz TJ, Shanks BH, Dumesic JA (2012) Triacetic acid lactone as a potential biorenewable platform chemical. Green Chem 14:1850–1853. https://doi.org/10.1039/C2GC35343A
22. Arnold F, Bürger V, Droste-Fanke B, Grimm F, Krieger A, Schneider J, Stilp T (1997) Acetone in the upper troposphere and lower stratosphere: impact on trace gases and aerosols. Geophys Res Lett 24:3017–3020. https://doi.org/10.1029/97GL02974
23. Ziemann PJ, Atkinson R (2012) Kinetics, products, and mechanisms of secondary organic aerosol formation. Chem Soc Rev 41:6582–6605. https://doi.org/10.1039/C2CS35122F
24. Perring A, Pusede S, Cohen R (2013) An observational perspective on the atmospheric impacts of alkyl and multifunctional nitrates on ozone and secondary organic aerosol. Chem Rev 113:5848–5870. https://doi.org/10.1021/cr300520x
25. Wang C, Wania F, Goss K-U (2018) Is secondary organic aerosol yield governed by kinetic factors rather than equilibrium partitioning? Environ Sci Process Impacts 20:245–252. https://doi.org/10.1039/C7EM00451F
26. Hehre W, Radom L, Schleyer PR, Pople JA (1986) Ab initio molecular orbital theory. Wiley, New York
27. Becke AD (1993) A new mixing of Hartree-Fock and local density-functional theories. J Chem Phys 98:1372–1377. https://doi.org/10.1063/1.464304
28. Dunning TH Jr (1989) Gaussian basis sets for use in correlated molecular calculations. I. The atoms boron through neon and hydrogen. J Chem Phys 90:1007–1023. https://doi.org/10.1063/1.456153
29. Gour NK, Gupta S, Mishra BK, Singh HJ (2014) A computational study on kinetics, mechanism, and thermochemistry of gas-phase reactions of 3-hydroxy-2-butanone with OH radicals. J Chem Sci 126:1789–1801. https://doi.org/10.1007/s12039-014-0733-6
30. Priya AM, El Dib G, Senthilkumar L, Sleiman C, Tomas A, Canosa A, Chakir A (2015) An experimental and theoretical study of the kinetics of the reaction between 3-hydroxy-3-methyl-2-butanone and OH radicals. RSC Adv 5:26559–26568. https://doi.org/10.1039/C4RA15664A
31. Guleria K, Subramanian R (2022) Theoretical study of mechanisms and kinetics of reactions of the $O(^3P)$ atom with alkyl hydroperoxides (ROOH) where ($R=CH_3$ & C_2H_5). Comput Theor Chem 1208:113547. https://doi.org/10.1016/j.comptc.2021.113547
32. Helgaker T, Klopper W, Koch H, Noga J (1997) Basis-set convergence of correlated calculations on water. J Chem Phys 106:9639–9646. https://doi.org/10.1063/1.473863
33. Halkier A, Helgaker T, Jørgense P, Klopper W, Koch H, Olsen J, Wilson AK (1998) Basis-set convergence in correlated calculations on Ne, N_2, and H_2O. Chem Phys Lett 286:243–252. https://doi.org/10.1016/S0009-2614(98)00111-0
34. Gonzalez C, Schlegel HB (1989) An improved algorithm for reaction path following. J Chem Phys 90:2154–2161. https://doi.org/10.1063/1.456010
35. Gonzalez C, Schlegel HB (1990) Reaction path following in mass-weighted internal coordinates. J Phys Chem 94:5523–5527. https://doi.org/10.1021/j100377a021
36. Pople JA, Head-Gordon M, Raghavachari K (1987) Quadratic configuration interaction. A general technique for determining electron correlation energies. J Chem Phys 87:5968–5975. https://doi.org/10.1063/1.453520
37. Lee TJ, Taylor PR (1989) A diagnostic for determining the quality of single-reference electron correlation methods. Int J Quantum Chem 36:199–207. https://doi.org/10.1002/qua.56036084
38. Rienstra-Kiracofe JC, Allen WD, Schaefer HF (2000) The $C_2H_5 + O_2$ reaction mechanism: high-level ab initio characterizations. J Phys Chem A 104:9823–9840. https://doi.org/10.1021/jp001041k
39. Dennington R, Keith T, Millam JG (2009) Version 5 Semichem Inc. Shawnee Mission KS
40. Frisch M, Trucks G, Schlegel H, Scuseria G, Robb M, Cheeseman J, Scalmani G, Barone V, Petersson G, Nakatsuji H (2016) Gaussian 16, Revision A03 Gaussian Inc, Wallingford
41. Zheng J, Bao JR, Meana-Pañeda R, Zhang S, Lynch GC, Corchado JC, Chuang YY, Fast PL, Hu WP, Liu YP et al (2018) Polyrate 2017-C. University of Minnesota, Minneapolis, MN
42. Garrett BC, Truhlar DG (1979) Generalized transition state theory. Bond energy-bond order method for canonical variational calculations with application to hydrogen atom transfer reactions. J Am Chem Soc 101:4534–4548. https://doi.org/10.1021/ja00510a019
43. Garrett BC, Truhlar DG (1979) Criterion of minimum state density in the transition state theory of bimolecular reactions. J Chem Phys 70:1593–1598. https://doi.org/10.1063/1.437698
44. Garrett BC, Truhlar DG, Grev RS, Magnuson AW (1980) Improved treatment of threshold contributions in variational transition-state theory. J Phys Chem 84:1730–1748. https://doi.org/10.1021/j100450a013
45. Kuppermann A, Truhlar DG (1971) Exact tunneling calculations. J Am Chem Soc 93:1840–1851. https://doi.org/10.1021/ja00737a002
46. Fernandez-Ramos A, Ellingson BA, Garrett BC, Truhlar DG (2007) Variational transition state theory with multidimensional tunneling. Rev Comput Chem 23:125–232. https://doi.org/10.1002/9780470116449.ch3
47. Truhlar DG, Isaacson AD, Garrett BC (1985) Generalized transition state theory. Theory Chem React Dyn 4:65–137
48. Isaacson AD, Truhlar DG, Rai SN, Steckler R, Hancock GC, Garrett BC, Redmon MJ (1987) POLYRATE: a general computer program for variational transition state theory and semiclassical tunneling calculations of chemical reaction rates. Comput Phys Commun 47:91–102. https://doi.org/10.1016/0010-4655(87)90069-5
49. Lu D, Truong TN, Melissas VS, Lynch GC, Liu Y-P, Garrett BC, Steckler R, Isaacson AD, Rai SN, Hancock GC (1992) Polyrate 4: a new version of a computer program for the calculation of

chemical reaction rates for polyatomics. Comput Phys Commun 71:235–262. https://doi.org/10.1016/0010-4655(92)90012-N
50. Liu YP, Lynch GC, Truong TN, Lu DH, Truhlar DG, Garrett B (1993) Molecular modeling of the kinetic isotope effect for the [1,5]-sigmatropic rearrangement of cis-1,3-pentadiene. J Am Chem Soc 115:2408–2415. https://doi.org/10.1021/ja00059a041
51. Srinivasulu G, Vijayakumar S, Rajakumar B (2018) Kinetic Investigations on the gas phase reaction of 2,2, 2-trifluoroethylbutyrate with OH radicals: an experimental and theoretical study. ChemistrySelect 3:4480–4489. https://doi.org/10.1002/slct.201703113
52. Dib GE, Aazaad B, Lakshmipathi S, Laversin H, Roth E, Chakir A (2018) An experimental and theoretical study on the kinetics of the reaction between 4-hydroxy-3-hexanone $CH_3CH_2C(O)CH(OH)CH_2CH_3$ and OH radicals. Int J Chem Kinet 50:556–567. https://doi.org/10.1002/kin.21181
53. Priya AM, Lakshmipathi S, Chakir A, El Dib G (2016) First experimental and theoretical kinetic study of the reaction of 4-hydroxy-4-methyl 2-pentanone as a function of temperature. Int J Chem Kinet 48:584–600. https://doi.org/10.1002/kin.21017
54. Skodje RT, Truhlar DG, Garrett BC (1982) Vibrationally adiabatic models for reactive tunneling. J Chem Phys 77:5955–5976. https://doi.org/10.1063/1.443866
55. Truhlar DG, Brown FB, Steckler R, Isaacson AD (1986) The representation and use of potential energy surfaces in the wide vicinity of a reaction path for dynamics calculations on polyatomic reactions. Theory of chemical reaction dynamics. Springer, pp 285–329
56. Truhlar DG, Garrett BC (1987) Dynamical bottlenecks and semiclassical tunneling paths for chemical reactions. J Chim Phys 84:365–369. https://doi.org/10.1051/jcp/1987840365
57. Marcus R (1966) On the analytical mechanics of chemical reactions. Quantum mechanics of linear collisions. J Chem Phys 45:4493–4499. https://doi.org/10.1063/1.1727528
58. Truhlar DG, Garrett BC (1984) Variational transition state theory. Annu Rev Phys Chem 35:159–189. https://doi.org/10.1146/annurev.pc.35.100184.001111
59. Marcus R, Coltrin ME (1977) A new tunneling path for reactions such as $H + H_2 \rightarrow H_2 + H$. J Chem Phys 67:2609–2613. https://doi.org/10.1063/1.435172
60. Skodje RT, Truhlar DG, Garrett BC (1981) A general small-curvature approximation for transition-state-theory transmission coefficients. J Phys Chem 85:3019–3023. https://doi.org/10.1021/j150621a001
61. Moberly JG, Bernards MT, Waynant KV (2018) Key features and updates for Origin 2018. J Cheminformatics 10:1–2. https://doi.org/10.1186/s13321-018-0259-x
62. Flynn J (1990) Temperature dependence of the rate of reaction in thermal analysis: the Arrhenius equation in condensed phase kinetics. J Therm Anal Calorim 36:1579–1593. https://doi.org/10.1007/bf01914077
63. Guleria K, Subramanian R (2022) Quantum chemical and chemical kinetic investigation on hydrogen abstraction reactions of $CF_3CF_2C(O)OCH_3$ and $CHF_2CF_2C(O)OCH_3$ with OH radicals and fate of haloalkoxy radicals. ACS Earth Space Chem 6:1596–1611. https://doi.org/10.1021/acsearthspacechem2c00069
64. Hammond GS (1955) A correlation of reaction rates. J Am Chem Soc 77:334–338. https://doi.org/10.1021/ja01607a027
65. Aslan L, Laversin H, Coddeville P, Fittschen C, Roth E, Tomas A, Chakir A (2017) Kinetics of the photolysis and OH reaction of 4-hydroxy-4-methyl-2-pentanone: atmospheric implications. Atmos Environ 150:256–263. https://doi.org/10.1016/j.atmosenv.2016.11.059
66. Wallington TJ, Kurylo MJ (1987) Flash photolysis resonance fluorescence investigation of the gas-phase reactions of hydroxyl radicals with a series of aliphatic ketones over the temperature range 240–440 K. J Phys Chem 91:5050–5054. https://doi.org/10.1021/j100303a033
67. Alvarez-Idaboy JR, Cruz-Torres A, Galano A, Ruiz-Santoyo ME (2004) Structure-reactivity relationship in ketones + OH reactions: a quantum mechanical and TST approach. J Phys Chem A 108:2740–2749. https://doi.org/10.1021/jp036795o
68. Baasandorj M, Griffith S, Dusanter S, Stevens PS (2009) Experimental and theoretical studies of the kinetics of the OH + hydroxyacetone reaction as a function of temperature. J Phys Chem A 113:10495–10502. https://doi.org/10.1021/j100303a033
69. Galano A (2006) Theoretical study on the reaction of tropospheric interest: hydroxyacetone + OH. Mechanism and kinetics. J Phys Chem A 110:9153–9160. https://doi.org/10.1021/jp061705b
70. Gao Y, Zhao Y, Guan Q, Wang F (2020) Ab initio kinetics predictions for the role of pre-reaction complexes in hydrogen abstraction from 2-butanone by OH radicals. RSC Adv 10:33205–33212. https://doi.org/10.1039/D0RA05332E
71. Atkinson R, Tuazon EC, Aschmann SM (2000) Atmospheric chemistry of 2-pentanone and 2-heptanone. Environ Sci Technol 34:623–631. https://doi.org/10.1021/es9909374
72. Zhang S, Sun J, Cao H, Qiao Q, He M (2017) Computational study on the mechanism and kinetics of Cl-initiated oxidation of ethyl acrylate. Struct Chem 28:1831–1842. https://doi.org/10.1007/s11224-017-0967-2
73. Ji Y, Zheng J, Qin D, Li Y, Gao Y, Yao M, Chen X, Li G, An T, Zhang R (2018) OH-initiated oxidation of acetylacetone: implications for ozone and secondary organic aerosol formation. Environ Sci Technol 52:11169–11177. https://doi.org/10.1021/acs.est.8b03972
74. Colmenar I, Martin P, Cabanas B, Salgado S, Martinez E (2018) Analysis of reaction products formed in the gas phase reaction of E, E-2,4-hexadienal with atmospheric oxidants: reaction mechanisms and atmospheric implications. Atmos Environ 176:188–200. https://doi.org/10.1016/j.atmosenv.2017.12.027
75. Paul S, Gour NK, Deka RC (2019) Oxidation pathways, kinetics and branching ratios of chloromethyl ethyl ether (CMEE) initiated by OH radicals and the fate of its product radical: an insight from a computational study. Environ Sci Process Impacts 21:1519–1531. https://doi.org/10.1039/C9EM00104B
76. Hein R, Crutzen PJ, Heimann M (1997) An inverse modeling approach to investigate the global atmospheric methane cycle. Glob Biogeochem Cycles 11:43–76. https://doi.org/10.1029/96GB03043